

Mechanical Properties of Surfactant Bilayer Membranes from Atomistic and Coarse-Grained Molecular Dynamics Simulations

E. S. Boek^{*,†} and J. T. Padding[†]

Schlumberger Cambridge Research, High Cross, Madingley Road, Cambridge CB3 0EL, United Kingdom

W. K. den Otter and W. J. Briels[†]

Computational Dispersion Rheology, University of Twente, P.O. Box 217, 7500 AE Enschede, The Netherlands

Received: August 5, 2005

We use simulations to predict the stability and mechanical properties of two amphiphilic bilayer membranes. We carry out atomistic MD simulations and investigate whether it is possible to use an existing coarse-grained (CG) surfactant model to map the membrane properties. We find that certain membranes can be represented well by the CG model, whereas others cannot. Atomistic MD simulations of the erucate membrane yield a headgroup area per surfactant a_0 of 0.26 nm², an elastic modulus K_A of 1.7 N/m, and a bending rigidity κ of 5 $k_B T$. We find that the CG model, with the right choice for the size and potential well depth of the head, correctly reproduces a_0 , κ , as well as the fluctuation spectrum over the whole range of q values. Atomistic MD simulations of EHAC, on the other hand, suggest that this membrane is unstable. This is indicated by the fact that κ is of the order of $k_B T$, which means that the interface is extremely flexible and diffuse, and K_A is close to zero, which means that the surface tension is zero. We argue that the CG model can be used if the headgroups are uncharged, dipolar, or effectively dipolar due to headgroup charge screening induced by counterion condensation.

I. Introduction

Surfactant molecules may spontaneously self-assemble into a variety of ordered phases of both academic and practical interest. An example of the latter is that in hydrocarbon recovery processes, there is increasing need for responsive fluids which can transform their characteristics from low viscosity, Newtonian behavior to a highly viscoelastic gel, then back to a low viscosity liquid. This is required at different stages of a reservoir treatment process in response to chemical or physical triggers that either occur naturally in the process or can be imposed externally. Surfactant self-assembly and disassembly is one route for achieving this, and viscoelastic surfactants operating in the wormlike micelle regime are being increasingly used as reservoir stimulation fluids.¹ Under certain conditions, the membrane phase may be important when considering the flow of these viscoelastic surfactant fluids in confined geometries such as porous media.² More generally, surfactant bilayers are important in biological tissues such as cell membranes.

Computer simulation has evolved as a useful tool to study bilayer membranes. Properties examined include, among others, self-assembly,^{3,4} interfacial tension,^{5–7} area compressibility and bending rigidity,^{6–9} and the edge free energy of a pore.¹⁰

In this paper, we investigate the mechanical properties of two different surfactant bilayer membranes, the structures of which will be described below. For this purpose, we use MD simulations at two different levels. At the first level, we describe the surfactants in full atomistic detail. The advantage of this method is that the chemistry of the surfactants is represented

explicitly. The disadvantage, however, is that simulations at this level are computationally demanding. Therefore they are limited to relatively small length and time scales. For this reason, it is attractive to consider coarse-grained (CG) models, in which only the essential details of a surfactant molecule are retained. In its simplest representation, an amphiphile molecule consists of a hydrophilic head and a hydrophobic tail. Computer simulations by Smit et al.¹⁵ have shown that such a simple model captures essential aspects of micelle formation at interfaces. A slightly extended CG amphiphile simulation model was developed by Goetz et al.³ In this model, the tail is represented by four beads, to account for the excluded volume and degrees of freedom of the tail. It appears that the general mechanical properties of membranes, such as compressibility and bending rigidity, are well represented by this extended model.^{8,9} However, it is not clear a priori whether the properties of the CG model can be mapped onto those of a specific surfactant membrane. In this paper, we will investigate this and show that this mapping is possible for certain amphiphilic bilayers. Note that our approach is different from other coarse-graining procedures in the literature, where the interactions between the CG beads are determined *bottom-up* from atomistic simulations.^{16–18} Very recently, a promising CG model for lipid MD simulations along these lines was described by Marrink et al.,¹⁹ successfully mapping various structural, dynamical, and mechanical properties of membranes. Although this bottom-up approach appears to be successful, it has two disadvantages. First, it should be realized that it is nontrivial to determine CG parameters from atomistic models.^{18,20} Second, the CG models produced are not general but apply to a specific surfactant. Therefore the CG procedure needs to be repeated for every amphiphile considered. In this paper, we will show, for the first time, that it is possible

* Address correspondence to this author. E-mail: boek@cambridge.oilfield.slb.com.

[†] Also at Department of Chemistry, University of Cambridge, Lensfield Road, Cambridge, U.K.

to map the mechanical properties of a specific amphiphilic membrane using the simple *top-down* approach of Goetz et al.³

II. Theory

The free energy F of a nearly flat bilayer membrane $z(x,y)$ with area A is given by the Helfrich expression²⁵ as a sum of bending and stretching contributions,

$$F = \frac{1}{2} \kappa \iint \left(\frac{\partial^2 z}{\partial x^2} + \frac{\partial^2 z}{\partial y^2} \right)^2 dx dy + \frac{K_A}{2A_0} (A - A_0)^2 \quad (1)$$

Here κ is the bending rigidity, A_0 the equilibrium area, and K_A the elastic modulus. It is our objective to calculate these parameters for our model.

Consider a rectangular bilayer oriented along the xy direction in a box of dimensions $L_x \neq L_y \neq L_z$. If the dimensions of the box are changed, while conserving its total volume, it can be shown, following ref 9, that the free energy of the system changes by

$$\frac{1}{L_y} \left(\frac{\partial F}{\partial L_x} \right)_{L_y, V} + \frac{1}{L_x} \left(\frac{\partial F}{\partial L_y} \right)_{L_x, V} = L_z (2p_{zz} - (p_{xx} + p_{yy})) = 2 \frac{K_A}{A_0} (A - A_0) \quad (2)$$

where p_{ii} are the diagonal elements of the stress tensor. Qualitatively, eq 2 can be explained as follows: for a three-dimensional liquid box, the pressure is isotropic so that the free energy is independent of the box dimensions (at constant volume); for a box containing a membrane, however, the ordering of the particles in and near the membrane, and therefore the free energy, will change upon a deformation of the box. The value of the elastic modulus K_A can be determined from simulations using eq 2.

We describe the bilayer midplane in the Monge representation²⁵ by $z(x,y)$. Because of the periodicity imposed on the bilayer by the periodic boundary conditions, the midplane of the bilayer membrane is expressed as a Fourier series

$$z(x,y) = \sum_{n_x} \sum_{n_y} c_{n_x, n_y} \exp \left[2\pi i \left(n_x \frac{x}{L_x} + n_y \frac{y}{L_y} \right) \right] + z_0 \quad (3)$$

where L_x and L_y are the dimensions of the membrane in x and y directions, respectively, and $z_0 = N^{-1} \sum_i z_i$. To determine the bending rigidity κ , we calculate the static structure factor $S(\mathbf{q})$. In the following, we will use both structure factor and fluctuation spectrum as interchangeable terms to indicate $S(\mathbf{q})$. For a tensionless membrane, the equipartition theorem yields

$$S(\mathbf{q}) = \langle c_n c_n^* \rangle = \frac{k_B T}{\kappa L_x L_y} q^{-4} \quad (4)$$

with wave vector

$$\mathbf{q} = 2\pi \left(\frac{n_x}{L_x}, \frac{n_y}{L_y} \right) \quad (5)$$

Equation 3 can be formally inverted to express c_n as an integral of the perpendicular coordinate z . Substituting the smooth plane by a series of Dirac delta peaks centered on the atoms in the bilayer,

$$z(x,y) \rightarrow \frac{L_x L_y}{N} \sum_{i=1}^N z_i \delta(x - x_i) \delta(y - y_i) \quad (6)$$

and integrating over x and y , we find

$$c_n = \frac{1}{N} \sum_{i=1}^N (z_i - z_0) \exp \left[-2\pi i \left(n_x \frac{x_i}{L_x} + n_y \frac{y_i}{L_y} \right) \right] \quad (7)$$

Now we can verify whether the distributions observed in the simulations are in agreement with the prediction of eq 4. If this is the case, then we can extract a value for the bending rigidity κ . This method of calculating κ was successfully used by Goetz et al.⁸ and den Otter and Briels⁹ for coarse-grained membranes. Recently, atomistic membranes have been studied in this fashion by Lindahl and Edholm⁶ and Marrink and Mark.⁷

III. Surfactants

In our studies, two types of surfactants were investigated which differ only in their hydrophilic headgroup chemistry. They have the same hydrophobic part, $\text{CH}_3(\text{CH}_2)_7\text{CH}=\text{CH}(\text{CH}_2)_{12}$, which is a linear hydrocarbon chain $\text{C}_{22}\text{H}_{43}$ with a *cis*-double bond between the 9th and 10th carbon atoms (the atoms are counted from the CH_3 group). These surfactants have ionic headgroups of the following types: erucate, anionic surfactant with a negatively charged carboxylate headgroup ($-\text{COO}^-$) and sodium counterion, and EHAC, cationic surfactant with a positively charged $-\text{N}^+(\text{CH}_2\text{CH}_2\text{OH})_2\text{CH}_3$ (bis(hydroxyethyl)-methylammonium) headgroup and chloride counterion.

Note that both surfactant systems are currently being used for hydraulic fracturing operations in hydrocarbon recovery.^{11,21} These surfactants typically assemble into wormlike micelles at low surfactant concentrations and form viscoelastic gels.²² One of the concerns for application purposes is whether these amphiphiles assemble into a *lamellar* phase at sufficiently high surfactant concentrations.²³ We believe that it is possible that lamellar phases will form in porous media flow, where the surfactants tend to concentrate in constrictions due to adsorption and exclusion effects. At the time when our research was carried out, we did not have direct experimental evidence for the stability of the lamellar phases of these particular compounds.²⁴ One of the purposes of this study is to use computer simulations to *predict* the stability and mechanical properties of the two amphiphilic bilayer membranes. Snapshots of the erucate and EHAC membranes¹¹ are shown in Figures 1 and 2, respectively.

IV. MD Simulation Details

Our simulations were performed using the DL_POLY²⁶ program package running in parallel under the MPI environment. One set of simulations was done with the Gromacs MD code²⁸ to compare the results for different force fields for bonded and nonbonded van der Waals interactions. The MOPAC²⁷ program package was used to perform geometry optimization and to calculate atomic charges of the surfactants. The resulting charges have been listed in a previous paper.¹¹ An orthogonal simulation box was used together with periodic boundary conditions in three dimensions. The surfactant bilayer, constructed by putting the surfactants tail-to-tail on a square lattice, was positioned in the middle of the box. The rest of the box was filled with SPC water molecules²⁹ and counterions. Two EHAC bilayer membranes were constructed, containing 128 ($8 \times 8 \times 2$, DL_POLY) and 242 ($11 \times 11 \times 2$, Gromacs) surfactant molecules, indicated by EHAC-128 and EHAC-242, respectively. Two erucate bilayer membranes were constructed, containing 128 ($8 \times 8 \times$

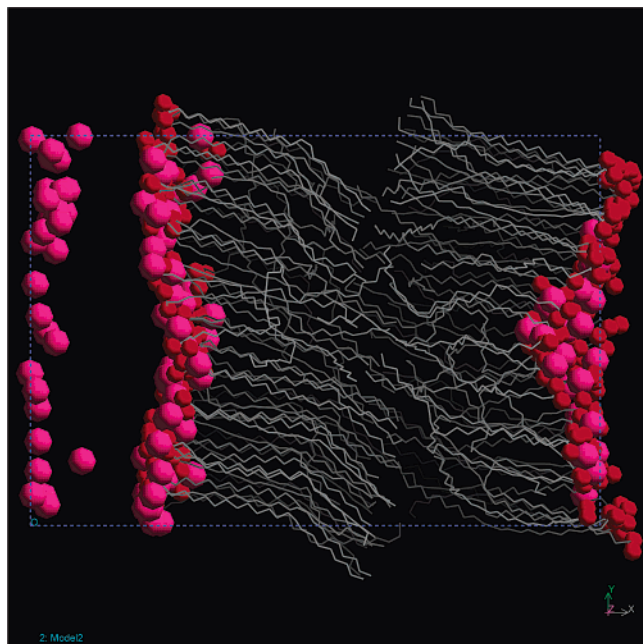


Figure 1. Simulation snapshot of headgroups, tails, and counterions for the erucate membrane.

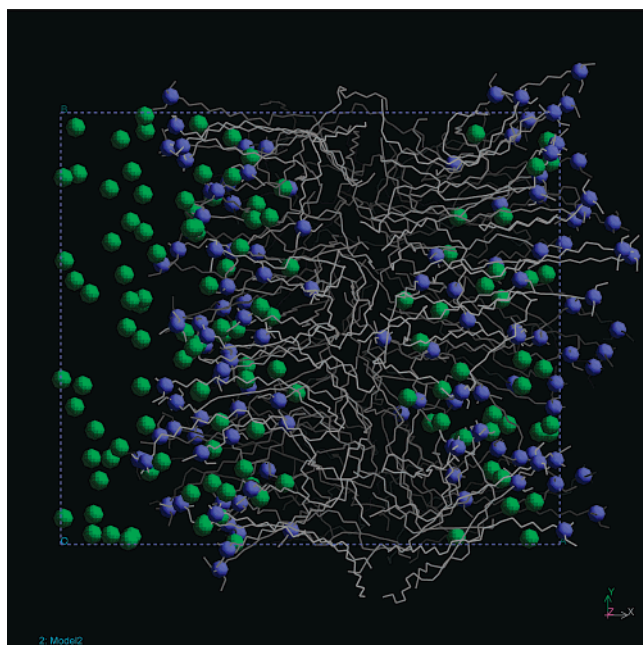


Figure 2. Simulation snapshot of headgroups, tails, and counterions for the EHAC membrane.

2, DL_POLY) and 256 ($16 \times 8 \times 2$, DL_POLY) surfactant molecules, indicated by erucate-128 and erucate-256, respectively. The number of water molecules was up to several thousands (see Table 1). The Ewald summation method was used to handle long-range Coulomb interactions. The equations of motion were integrated by using a Verlet leapfrog scheme³⁰ and a time step of 2 fs. The systems were first allowed to equilibrate in the constant (NVT) ensemble. The temperature was maintained at 300 K using an NVT –Nosé–Hoover thermostat.³¹ Subsequent simulations were carried out in the isothermal–isobaric (NpT) ensemble until the box dimensions were equilibrated. The pressure was maintained constant by using a Melchionna modification of the Hoover algorithm³² in which the equations of motion involve a Nosé–Hoover ther-

TABLE 1: Details of the Atomistic Membrane Simulation Boxes in the Tensionless State^a

label	no. of surf.	no. of water	A (nm ²)	a_0 (nm ²)	L_{\perp} (nm)
erucate-128	128	1106	16.62	0.26	7.64
erucate-256	256	2212	32.61	0.25	7.78
EHAC-128	128	1966	31.24	0.49	5.16
EHAC-242	242	3816	50.89	0.42	5.99

^a The area and thickness of the membrane are indicated by A_{\parallel} and L_{\perp} , respectively. The area per headgroup is indicated as a_0 . The number of surfactant and water molecules are indicated by no. of surf. and no. of water, respectively.

mostat and a barostat in the same spirit. The equilibrium state was determined by monitoring the size of the basic cell. Subsequently, the tensionless state was found by using a box scaling procedure described in section V.A. The details of the simulation boxes in the tensionless state are listed in Table 1. To examine whether the degree of hydration is sufficient, we make a comparison with the case of lipid DPPC membranes.¹⁹ In the case of DPPC it has been shown that full hydration requires 25 water molecules per surfactant. In our case, a smaller degree of hydration is sufficient to achieve the same thickness of the water layer, taking into account the smaller headgroup area a_0 of our surfactants (Table 1) compared with that of DPPC ($a_0 = 0.64$ nm²).

V. Results

We will first discuss the atomistic membranes, followed by the coarse-grained membranes.

A. Atomistic Membranes. Figure 1 shows that the erucate membrane is highly structured on the time scale of the simulation. The counterions are condensed on the membrane surface, as observed from structural simulation properties in ref 11. The condensation leads to an effective screening of the repulsive headgroup interactions. Figure 2, on the other hand, shows that the EHAC membrane is highly disordered and has a diffuse distribution of counterions. Additional evidence for these observations is given by the mean square displacements (msd) of the headgroups and the counterions, presented in Figure 3. This figure shows that both the lateral and perpendicular msd of the erucate counterions closely follow that of the erucate headgroups, whereas they are independent in the case of the EHAC counterions. Also, it can be seen that the diffusive motion is much smaller for the erucate than for the EHAC membrane counterions. The figure proves that the erucate headgroups still have some lateral diffusive motion. This means that the erucate membrane does not represent a crystalline phase, but a gel phase.¹⁹ Note that our observations are in agreement with recent DPD simulations of membranes, confirming that decreasing the head–head repulsion stabilizes the gel (L_{β}) phase, see refs 12 and 13. The EHAC membrane on the other hand displays significant diffusion perpendicular to the membrane. This indicates that the membrane fluctuates strongly and may even be unstable. We also measured the msd of the water molecules, see Figure 3. The msd in the direction perpendicular to the membrane goes, for both erucate and EHAC, asymptotically to a value of $d^2/6$, where d is the thickness of the water layer. This is in agreement with theoretical expectations. The lateral diffusion coefficients for water in both the EHAC and erucate systems are of the order of 1 Å²/ps, in agreement with experiment.

It is important to note that eq 4 is only valid when the membrane is in a state of zero surface tension. To find the tensionless state, we used a box scaling procedure using a

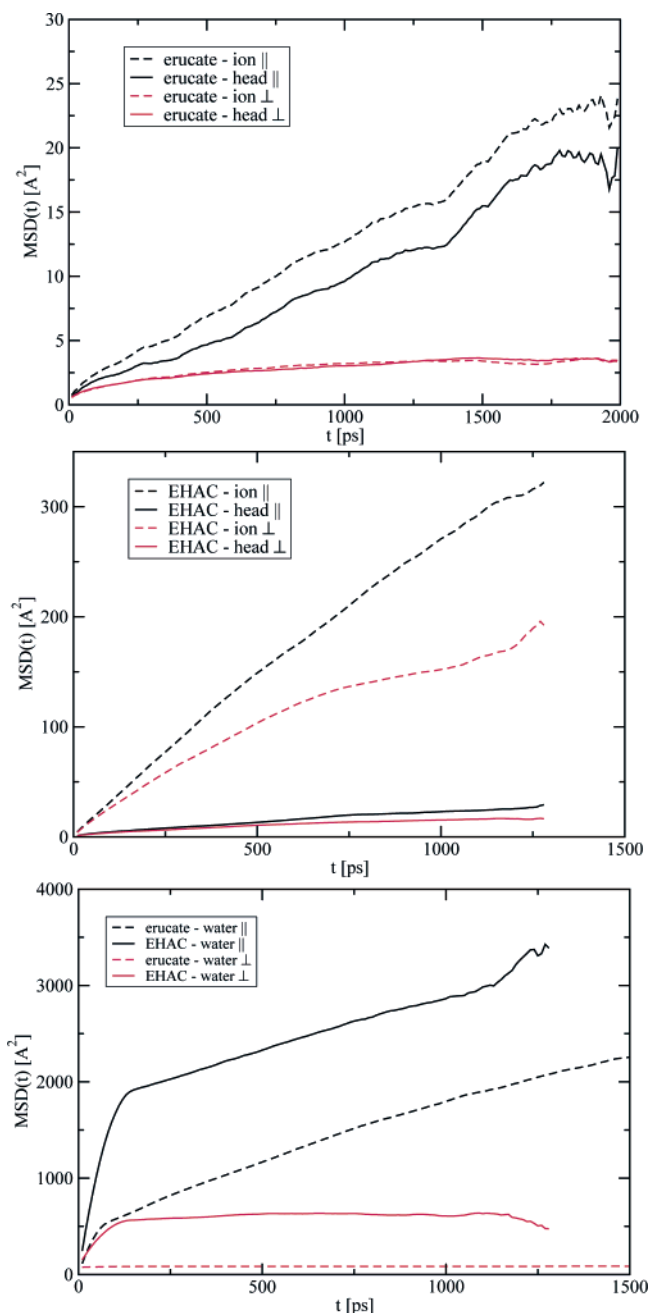


Figure 3. Mean square displacements for headgroups and ions for the erucate (top) and EHAC (middle) membranes, respectively. The water msd for both membranes is shown in the bottom graph.

modified Berendsen barostat (den Otter and Briels, ref 9), scaling L_x and L_y every time step by a factor proportional to the pressure difference

$$\delta p = p_{zz} - \frac{1}{2}(p_{xx} + p_{yy}) \quad (8)$$

The perpendicular dimension L_z was scaled simultaneously, keeping the total volume of the simulation box constant. In this fashion, reasonable estimates of the box dimensions of the tensionless states were obtained from simulations of roughly 0.5 ns. For the case of erucate, the area per headgroup in the small box is $a_0 = 0.26 \text{ nm}^2$ while the thickness of the surfactant bilayer is roughly 5.2 nm. To obtain a more accurate estimate, we carried out a number of simulations at fixed box sizes around the tensionless state. The lateral dimensions of the membrane

were stretched or compressed in a series of small steps with respect to the box dimensions determined above, while keeping the total volume of the simulation box constant. From subsequent simulations carried out at constant volume, the pressure difference was found to be proportional with the area of the bilayer, in agreement with eq 2. For the erucate-128 and EHAC-128 membranes, this is shown in Figure 4. We only show the smaller membrane results here, because the larger membranes will tend to buckle (see below and ref 33). For erucate, we find that the area per headgroup in the small box is $a_0 = 0.256 \text{ nm}^2$. The slope of this function then yields the area compressibility or elastic modulus K_A of the membrane, which was found from a linear fit to be 1.7 J m^{-2} . In the absence of experimental data for erucate bilayers, we note that this value is somewhat larger than that for atomistic (double tail) DPPC membrane simulations (0.3 J m^{-2}).⁶ This is possibly due to the tight packing of the erucate tails. For the EHAC membrane, the value of the pressure difference was found to be close to zero for every value of the area considered (see Figure 4). Therefore the area compressibility or elastic modulus K_A , as defined in eq 2, is close to zero. This result will be further discussed below. It also implies that the area per headgroup a_0 cannot be determined accurately. This explains the discrepancy between the values of a_0 in the two different boxes (see Table 1).

The membranes were run in the tensionless state for approximately 2 ns each. The Fourier transform of eq 7 was calculated every 50 steps. The resulting structure factors $S(\mathbf{q})$ of the erucate-256 membrane are shown in Figure 5 as a function of the length of the wave vector \mathbf{q} . We only show the $S(\mathbf{q})$ of the larger membranes here, because they produce the smallest \mathbf{q} modes.

Several features can be distinguished in the erucate fluctuation spectrum. A local maximum is observed at $q = 1.4 \text{ Å}^{-1}$, corresponding with a wavelength $2\pi/q = 4.5 \text{ Å}$. This value coincides with the location of the first peak in the radial distribution function for the erucate headgroups, corresponding with nearest neighbor distances between surfactants in one leaflet of the bilayer membrane, as shown in Figure 12 of ref 11. For smaller values of \mathbf{q} , the value of the structure factor increases, but it is not immediately clear whether the \mathbf{q}^{-4} behavior is recovered. This is due to the finite size of the membrane limiting the range of $S(\mathbf{q})$ to be observed for small \mathbf{q} . In the following section, we will give a motivated estimate of the bending modulus κ for the erucate membrane, by means of mapping on a coarse-grained surfactant model. The resulting value of $\kappa = 2.2 \times 10^{-20} \text{ J}$ is in good general agreement with that of a DPPC membrane with a value of $\kappa = 4 \times 10^{-20} \text{ J}$.⁶

The fluctuation spectra for EHAC membranes with use of both the DL_POLY ($8 \times 8 \times 2$) and Gromacs ($11 \times 11 \times 2$) MD codes are presented in Figure 6. It is interesting to observe that these spectra display very similar behavior. This can be explained by realizing that the Coulomb part of the nonbonded interactions is the same for both models. Apparently, the different models for bonded and van der Waals interactions are unimportant in this respect, as is the effect of different membrane sizes used. This indicates that the fluctuation spectrum has general properties, largely independent of force field or system size used. Assuming that the lowest \mathbf{q} modes satisfy the \mathbf{q}^{-4} behavior, we have fitted a line to these points (see Figure 6). Using eq 4, we then find a value of the bending rigidity $\kappa = 0.7 k_B T$. The fact that κ is of the order of $1 k_B T$ suggests that the interface is extremely flexible and confirms our observation in Figure 2 that the EHAC membrane has a diffuse and

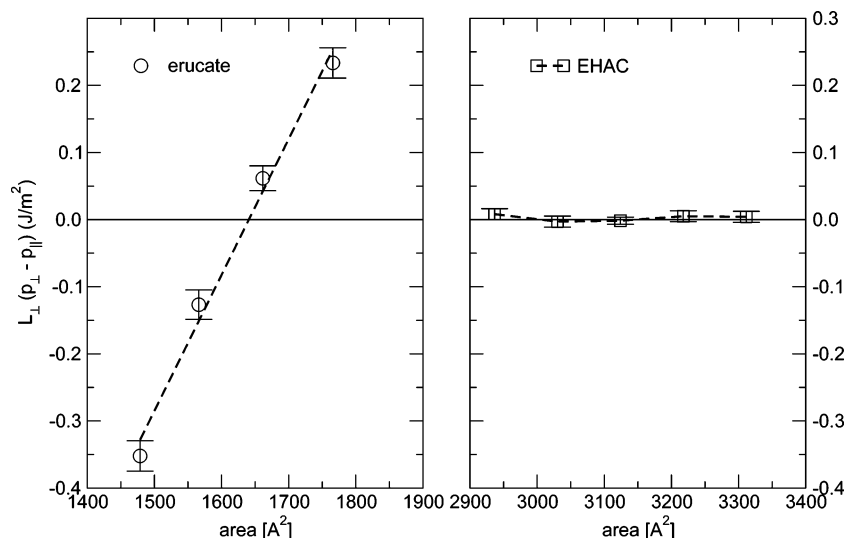


Figure 4. Difference between parallel and perpendicular pressures as a function of the area of the bilayer A in \AA^2 for the erucate-128 (left) and EHAC-128 (right) membranes.

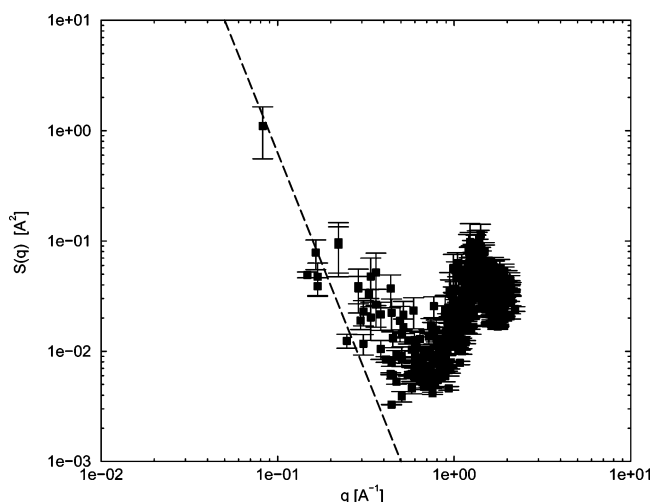


Figure 5. Structure factors for the tensionless atomistic erucate-256 membrane: a line following q^{-4} is added as a guide to the eye. See text for details.

disintegrated interface. This may indicate that this membrane is, in fact, unstable. We will further discuss this in the next section.

B. Coarse-Grained Membranes. To clarify the behavior for large wavelengths, we have performed membrane simulations for a coarse-grained model surfactant. Using this model, introduced by Goetz et al.,³ it is possible to study larger membranes at smaller computational cost than for the fully atomistic models. We will show that it is possible to map the mechanical properties of the coarse-grained model on that of one of the atomistic membranes. We only discuss the main features of the coarse-grained surfactant model here; for more detail we refer to the original paper.³ The surfactant consists of one head and four tail particles. The solvent particle is identical with the head particle. The hydrophobic interactions between tail and head or water particles are represented by a purely repulsive soft core potential:

$$\Phi_{\text{SC}}(r) = \epsilon \left(\frac{\sigma_{\text{SC}}}{r} \right)^9 \quad (9)$$

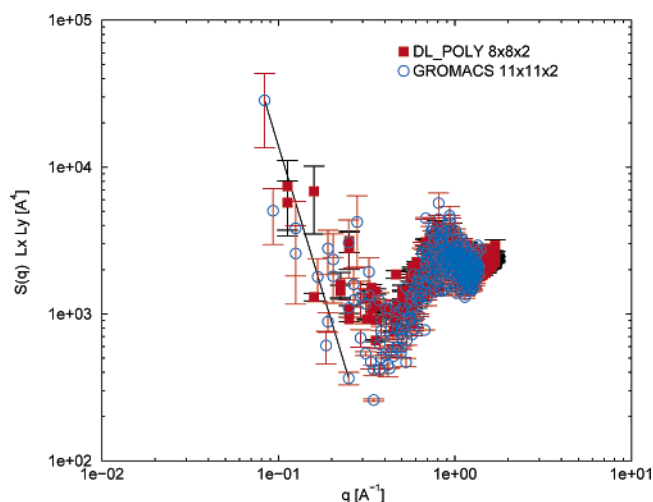


Figure 6. Structure factors for tensionless atomistic EHAC-128 and EHAC-242 membranes: comparison of DL_POLY and Gromacs simulations. A line following q^{-4} is added as a guide to the eye.

with $\sigma_{\text{SC}} = 1.05\sigma$. All other interactions are represented by a Lennard-Jones potential:

$$\Phi_{\text{LJ}}(r) = 4\epsilon \left[\left(\frac{\sigma}{r} \right)^{12} - \left(\frac{\sigma}{r} \right)^6 \right] \quad (10)$$

with $\sigma = 1/3$ nm and $\epsilon = 2$ kJ/mol. Both potentials are implemented in the shifted force fashion, such that both the value of the potential and its first derivative vanish at the cutoff distance $r_c = 2.5\sigma$. The head and tail particles are connected by a harmonic bond potential

$$\Phi_{\text{bond}}(l) = k_2(l - \sigma)^2 \quad (11)$$

with $k_2 = 5000\epsilon\sigma^{-2}$. To introduce a bending stiffness, we use an angle potential

$$\Phi_{\text{ang}}(\phi) = k_3[1 - \cos(\phi)] \quad (12)$$

where k_3 is the bending modulus of the semiflexible tails. In the simulations we use $k_3 = 2\epsilon$ or $k_3 = 5\epsilon$. There are no dihedral potentials. All particles have a mass m of 36 au, which combines with a particle density n of $2/3\sigma^3$ to yield a specific weight of

TABLE 2: Details of the Coarse-Grained Membrane Simulation Boxes in the Tensionless State^a

label	no. of surf.	no. of solvent	$A_{ }$ (nm ²)	a_0 (nm ²)	L_{\perp} (nm)
original CG	128	800	15.50	0.24	5.16
original CG	1152	10800	134.95	0.23	6.82
tuned CG	128	800	18.81	0.29	4.62
tuned CG	1152	10800	163.67	0.28	5.96

^a The original CG refers to the case $k_3 = 2\epsilon$, $\sigma_{\text{head}} = \sigma$, and $\epsilon_{\text{head}} = \epsilon$. The tuned CG model refers to the best match $k_3 = 2\epsilon$, $\sigma_{\text{head}} = 1.35\sigma$, and $\epsilon_{\text{head}} = 2\epsilon$. The area and thickness of the membrane are indicated by $A_{||}$ and L_{\perp} , respectively. The area per headgroup is indicated as a_0 . The number of surfactant molecules and solvent beads are indicated by no. of surf. and no. of solvent, respectively.

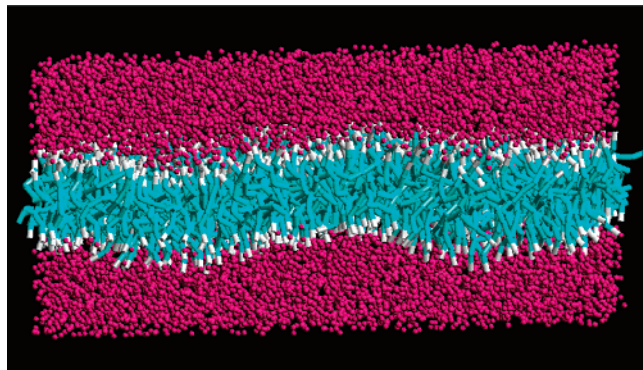


Figure 7. Snapshot of the coarse-grained bilayer membrane: red spheres, water; white cylinders, headgroups; and blue cylinders, surfactant tails.

1 g/cm³. The temperature is 325 K, or $1.35 \epsilon/k_B$, maintained by means of a Nosé-Hoover thermostat. A time step $\Delta t = t_{\text{sc}}/2000 = 0.7$ fs is used in the Verlet leapfrog scheme, where $t_{\text{sc}} = \sigma\sqrt{m/\epsilon}$ is the simulation scale. We use the DL_POLY MD code,²⁶ version 2.0.

Starting configurations were made by constructing two parallel layers of amphiphiles, heads pointing outward. The rest of the simulation box was filled randomly with solvent particles. After minimization and equilibration, simulations were performed to achieve the tensionless state, using the algorithm described above. Two simulation boxes, containing 128 and 1152 surfactants each, were created in this fashion. The details of the two simulation boxes in the tensionless state, as well as those of the fine-tuned CG model discussed below, are presented in Table 2.

The thickness of the solvent layer in the smaller CG box is similar to that used in the erucate box. The larger CG box requires a thicker water layer to accommodate the larger fluctuations of the bilayer, following eqs 3–5. Provided that the solvent layer is sufficiently thick, the results will not depend on the actual thickness of the water layer, as will be shown. A snapshot of the larger box is shown in Figure 7.

First of all, we performed a number of simulations around the tensionless states, as found in ref 9. The open squares in Figure 8 show that, for the small box, the pressure difference increases linearly with the area of the ground plane of the box. In the tension-free state the area per headgroup in the small box is $2.16 \sigma^2$ or 0.24 nm^2 , in excellent agreement with the value of $2.15 \sigma^2$ reported by Goetz and Lipowsky³ for the same system. A deviation from this value was found in a previous paper⁹ due to a mistake in the angle potential.³⁶ Furthermore, the area compressibility modulus of the small box was found to be $13.2 \epsilon\sigma^{-2}$ or 0.4 J m^{-2} , in good agreement with ref 9.

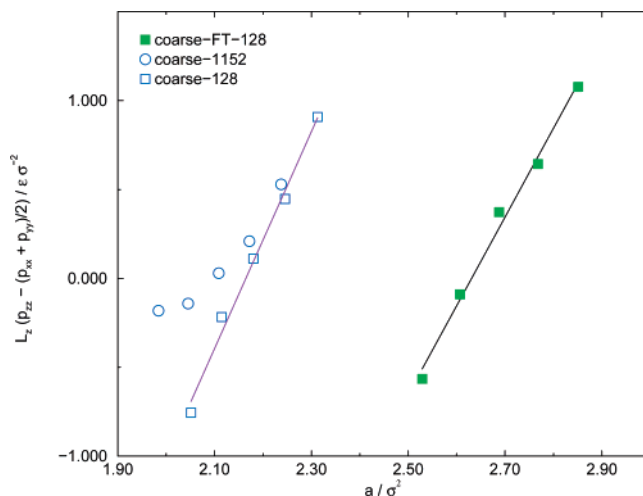


Figure 8. Difference between parallel and perpendicular pressures as a function of the relative area of the bilayer for the coarse-grained membranes. The open symbols indicate the original model (ref 9) for both small (coarse-128: circles) and large (coarse-1152: squares) membranes. The closed symbols indicate the fine-tuned model (coarse-FT-128). See text for details.

For the larger system, the pressure difference no longer decreases linearly with decreasing surface area of the box. This is due to buckling of the membrane at large system sizes.³³ Under strong compression forces, the bilayer prefers to bend rather than to further reduce its area, i.e. it buckles. This transition will occur in any bilayer, but is most easily observed in the large coarse-grained box because, following Euler's law,³⁴ the compression required to induce a transition decreases with increasing system size. The negative pressure difference (Figure 8) implies that the bilayer is in an unstable state, from which it can escape by reducing the difference between its real surface ($\approx A_{||}$) and the equilibrium surface $A_0 = Na_0$, where N is the number of surfactants. To achieve this, the system has two options:

(1) It can increase its area by bending. This can only be successful when the pressure difference is higher than a critical value, which depends on the system size, compressibility, and bending rigidity (in 2D the relation is given by the Euler formula).

(2) It can decrease A_0 . Because a_0 is fixed, this implies decreasing N , or dissolving a part of the bilayer.

However, the barrier for option 2 is so high that it is not an option in our simulation system (although under experimental conditions it should be possible, because a reduction of N lowers the free energy of the bent bilayer). Therefore, the first option is the only one.

Subsequently, we calculated the structure factors of the small and large coarse-grained membranes in the tensionless state, according to the method described above. The fluctuation spectra are shown in Figure 9 (closed symbols), together with the results for the atomistic membranes (open symbols). First, note that the results for the small and large CG boxes superimpose, even though the thickness of the solvent layer is different. This confirms that our solvent layer is sufficiently thick to accommodate fluctuations of the membrane. Second, it appears that, for large wavelengths, a linear regime is found with a slope of almost exactly minus four. This confirms that we are close to a state of vanishing surface tension. From the intercepts, reliable values of the bending rigidities can now be extracted. From Figure 9 it can already be observed qualitatively that the difference in headgroups results in a dramatic difference in the

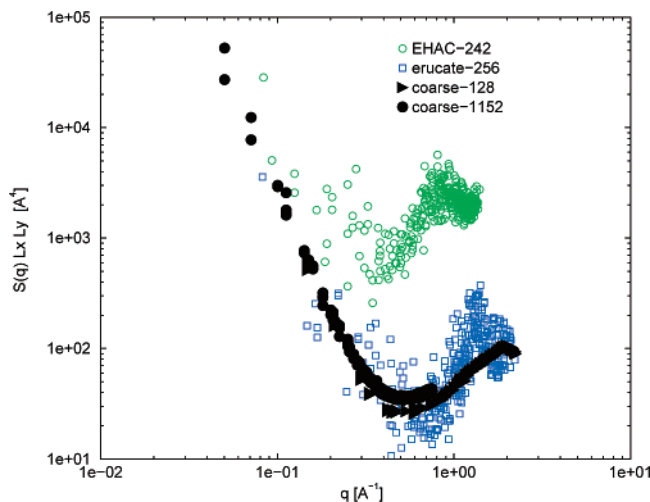


Figure 9. Structure factors for tensionless membranes: atomistic EHAC and erucate (open circles and squares, respectively) compared with the coarse-grained (Goetz et al.⁸) membranes, consisting of 128 and 1152 surfactants (closed triangles and circles respectively), using $k_3 = 2\epsilon$, $\sigma_{\text{head}} = \sigma$, and $\epsilon_{\text{head}} = \epsilon$.

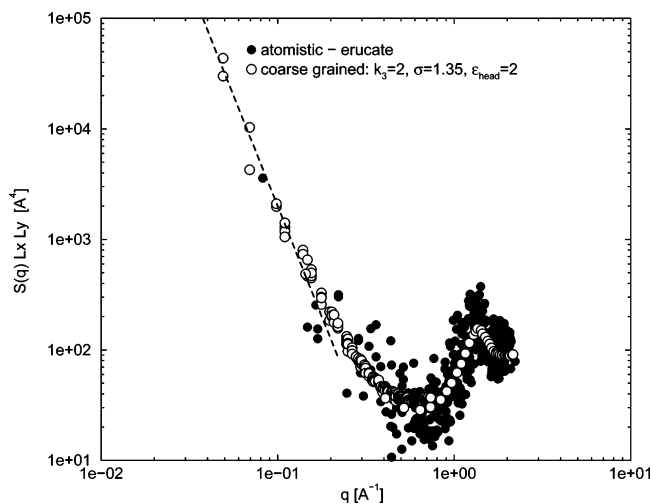


Figure 10. Structure factors for tensionless membranes: atomistic membrane (128 erucate molecules) compared with coarse-grained membranes (consisting of 128 and 1152 surfactants), using $k_3 = 2\epsilon$, $\sigma_{\text{head}} = 1.35\sigma$, and $\epsilon_{\text{head}} = 2\epsilon$. The dashed line is a q^{-4} fit.

fluctuation spectra of both atomistic membranes. We note that the amplitudes for EHAC are significantly higher than those for erucate, which implies that the EHAC membrane has a more strongly fluctuating interface than the erucate membrane. This is in qualitative agreement with our observations regarding the instability of the EHAC membrane in section V.A.

We will now investigate if it is possible to fine-tune the potential parameters of the coarse-grained model to yield fluctuation spectra that match the atomistic ones. As a criterion to optimize the fluctuation spectra for extrapolation to small q , we require that the spectrum should fit over the whole range of q . We systematically varied the headgroup size σ_{head} and potential well depth ϵ_{head} , as well as the bending modulus of the tails k_3 . For the case of erucate, the best match was achieved for $k_3 = 2\epsilon$, $\sigma_{\text{head}} = 1.35\sigma$, and $\epsilon_{\text{head}} = 2\epsilon$. This is shown in Figure 10. From the intercept for the large box (1152 molecules) follows a bending rigidity of $\kappa = 5 k_B T$ (6.75ϵ) $= 2.2 \times 10^{-20}$ J for the coarse-grained erucate membrane. In the tension-free state, the area per headgroup was found to be significantly larger than the original CG model^{3,9} with a value of $2.63 \sigma^2$ or 0.29

nm^2 , as shown in Figure 8 (filled symbols). Note that this value is in agreement with the value of 0.26 nm^2 obtained from our atomistic erucate model. The area compressibility modulus K_A was found to be $13.1 \epsilon \sigma^{-2}$ or 0.4 J m^{-2} , very similar to the original CG model. Similarly, we have tried a systematic variation of the values of ϵ_{head} , σ_{head} , and k_3 to map onto the $S(q)$ of EHAC. This led to a variety of micellar shapes (membranes, spheres, worms, inverted micelles, ...) but not to a membrane with the desired $S(q)$. This suggests that the CG model cannot be used to describe the EHAC membrane.

VI. Discussion and Conclusion

In this paper, we have used simulations to predict the stability and mechanical properties of two amphiphilic bilayer membranes, for which no experimental data were available. At one level, we carried out atomistic MD simulations. At the other level, we have investigated whether it is possible to use an existing coarse-grained (CG) surfactant model³ to map the properties of atomistic membranes. The advantage of using the CG model is that much larger length and time scales can be achieved. We find that certain membranes can be represented well by the CG model, whereas others cannot.

Atomistic MD simulations of the erucate membrane yield a headgroup area per surfactant a_0 of 0.26 nm^2 , an elastic modulus K_A of 1.7 N/m , and a bending rigidity κ of $5 k_B T$. We found that the CG model, with the right choice for the size and potential well depth of the head bead, was able to correctly reproduce the headgroup area, bending rigidity, as well as the fluctuation spectrum over the whole range of q values. In a sense, this means that the CG model has also successfully reproduced the structure of the membrane; however, only coarse structural aspects, relating to positions of the headgroups, are addressed, so that the match between atomistic and coarse-grained membranes may not be perfect with respect to the membrane structure.

Atomistic MD simulations of EHAC, on the other hand, suggest that the EHAC membrane is unstable. For this membrane, we measured a bending rigidity κ of the order of $1 k_B T$, which means that the interface is extremely flexible and diffuse. This is confirmed by structural information¹¹ and simulation snapshots. We also measured that the elastic modulus K_A is close to zero, which means that the surface tension is zero, due to a poorly defined interface, and that the membrane is deformable as a three-dimensional homogeneous and isotropic medium. This information indicates that the EHAC membrane is unstable, and only resembles a bilayer because of confinement in a small simulation box. A larger box would probably lead to disintegration of the membrane. We found that the CG model, despite a systematic variation of the headgroup parameters, was unable to reproduce the fluctuation spectrum.

Summarizing, our simulations suggest that one surfactant (erucate) does form a stable lamellar phase whereas the other (EHAC) does not. This is not entirely surprising, given the much larger headgroup area of EHAC (see Table 1). Note that recent experiments, carried out after the simulations were completed, indeed indicate that EHAC will not form a stable lamellar phase. On the other hand, there are strong indications that erucate will form a stable lamellar phase.³⁵ Therefore, these experiments confirm our simulation results.

We will now explain why certain membranes can be described by the CG surfactant model, whereas others cannot. If the atomistic headgroup is uncharged or dipolar, the interactions are short-ranged and can be well represented by the CG model where only short-ranged interactions are included. Also,

when the headgroup charges are screened through counterion condensation, as is the case for erucate, the interactions are effectively dipolar and short-ranged. If, on the other hand, the headgroup charges are not screened, as is the case for EHAC, long-range electrostatic interactions, handled by the Ewald summation, are very important. In this case, the current short-ranged CG model cannot, and should not, be applied.

For this reason, it is necessary to further develop the CG model,³ including handling of long-range interactions and optimization with respect to the membrane structure. Here, we have only varied the σ and ϵ of the headgroup. It may prove more successful to modify other parameters of the coarse-grained surfactant model, such as the length of the tail. It seems to be promising to extend the existing CG models by incorporating double bonds in the surfactant tails, following the model proposed by Marrink et al.¹⁹ We are planning to do this soon.

Acknowledgment. We thank Geoff Maitland, Maddalena Venturoli, John Crawshaw, Arben Jusufi, Bob Prud'homme, and Hartmut Loewen for their contributions to this work.

References and Notes

- (1) Maitland, G. C. *Curr. Opin. Colloid Interface Sci.* **2000**, *5*, 301.
- (2) Cheikh, C.; Koper, G. *Phys. Rev. Lett.* **2003**, *91*, 156102.
- (3) Goetz, R.; Lipowsky, R. *J. Chem. Phys.* **1998**, *108*, 7397.
- (4) Maillet, J.-B.; Lachet, V.; Coveney, P. V. *Phys. Chem. Chem. Phys.* **1999**, *1*, 5277.
- (5) Lindahl, E.; Edholm, O. *J. Chem. Phys.* **2000**, *113*, 3882.
- (6) Lindahl, E.; Edholm, O. *Biophys. J.* **2000**, *79*, 426.
- (7) Marrink, S. J.; Mark, A. E. *J. Phys. Chem. B* **2001**, *105*, 6122.
- (8) Goetz, R.; Gompper, G.; Lipowsky, R. *Phys. Rev. Lett.* **1999**, *82*, 221.
- (9) den Otter, W. K.; Briels, W. J. *J. Chem. Phys.* **2003**, *118*, 4712.
- (10) Tolpekina, T. V.; den Otter, W. K.; Briels, W. J. *J. Chem. Phys.* **2004**, *121*, 12060.
- (11) Boek, E. S.; Jusufi, A.; Loewen, H.; Maitland, G. C. *J. Phys. Condens. Matter* **2002**, *14*, 9413.
- (12) Kranenburg, M.; Venturoli, M.; Smit, B. *Phys. Rev. E* **2003**, *67*, 060901.
- (13) Kranenburg, M.; Venturoli, M.; Smit, B. *J. Phys. Chem. B* **2003**, *107*, 11491.
- (14) Kuynova, R.; Caffrey, M. *Chem. Phys. Lipids* **2002**, *115*, 107–219.
- (15) Smit, B.; Hilbers, P. A. J.; Esselink, K.; Rupert, L. A. M.; van Os, N. M.; Schlijper, A. G. *Nature* **1990**, *348*, 624.
- (16) Shelley, J. C.; Shelley, M.; Reeder, R.; Bandyopadhyay, S.; Klein, M. L. *J. Phys. Chem. B* **2001**, *105*, 4464.
- (17) Venturoli, M.; Smit, B. *Phys. Chem. Commun.* **1999**, *10*, 1.
- (18) Kranenburg, M.; Nicolas, J.-P.; Smit, B. *Phys. Chem. Chem. Phys.* **2004**, *66*, 4142–4151.
- (19) Marrink, S. J.; de Vries, A. H.; Mark, A. E. *J. Phys. Chem. B* **2004**, *108*, 750–760.
- (20) Nielsen, S. O.; Lopez, C. F.; Srinivas, G.; Klein, M. L. *J. Phys. Condens. Matter* **2004**, *66*, R481–R512.
- (21) Boek, E. S.; den Otter, W. K.; Briels, W. J.; Iakovlev, D. *Philos. Trans. R. Soc. London* **2004**, *362*, 1625.
- (22) Couillet, I.; Hughes, T.; Maitland, G.; Candau, F.; Candau, S. J. *Langmuir* **2004**, *20*, 9541–9550.
- (23) Jönsson, B.; Lindman, B.; Holmberg, K.; Kronberg, B. *Surfactants and polymers in aqueous solution*; Wiley & Sons Ltd.: New York, 1998.
- (24) Recent experiments, carried out after the completion of our simulations, indicate that EHAC does indeed not form a stable lamellar phase (R. K. Prud'homme, private conversation).
- (25) Safran, S. *Statistical Thermodynamics of surfaces, interfaces and membranes*; Addison-Wesley: Reading, MA, 1994.
- (26) Smith, W.; Forester, T. *J. Mol. Graphics* **1996**, *14*, 136.
- (27) Stewart, J. J. P. MOPAC 6.0, QCPE No. 445, 1990.
- (28) Lindahl, E.; Hess, B.; van der Spoel, D. *J. Mol. Model.* **2001**, *7*, 306–317.
- (29) Berendsen, H. J. C.; Postma, J. P. M.; van Gunsteren, W. F.; Hermans, J. In *Intermolecular Forces*; Pullman, B., Ed.; Reidel: Dordrecht, The Netherlands, 1981.
- (30) Allen, M. P.; Tildesley, D. J. *Computer Simulation of Liquids*; Clarendon Press: Oxford, UK, 1987.
- (31) Hoover, W. G. *Phys. Rev. A* **1985**, *31*, 1695.
- (32) Melchionna, S.; Cicciotti, G.; Holian, B. L. *Mol. Phys.* **1993**, *78*, 533.
- (33) den Otter, W. K. *J. Chem. Phys.*, in press.
- (34) Landau, L. D.; Lifschitz, E. M. *Theory of Elasticity*; Pergamon Press: New York, 1964.
- (35) Prud'homme, R. K. Private communication.
- (36) They used $\Phi_{\text{ang}}(\phi) = 2\epsilon[1 + \cos(\phi)]$.